

High-Speed Ion Flow, Substorm Current Wedge, and Multiple Pi 2 Pulsations

20 December 1998

Prepared by

K. SHIODAWA, W. BAUMJOHANN,
G. HAERENDEL, and G. PASCHMANN
Max-Planck-Institut für Extraterrestrische Physik
Garching, Germany

J. F. FENNELL
The Aerospace Corporation
Los Angeles, CA

E. FRIIS-CHRISTENSEN
Danish Meteorological Institute
Copenhagen, Denmark

H. LÜHR
GeoForschungsZentrum
Telegrafenberg, Potsdam, Germany

G. D. REEVES
Los Alamos National Laboratory
Los Alamos, NM

C. T. RUSSELL
University of California
Los Angeles, CA

P. R. SUTCLIFFE
Hermanus Magnetic Observatory
Hermanus, South Africa

K. TAKAHASHI
Nagoya University
Toyokawa, Japan

Prepared for

SPACE AND MISSILE SYSTEMS CENTER
AIR FORCE MATERIEL COMMAND
2430 E. El Segundo Boulevard
Los Angeles Air Force Base, CA 90245

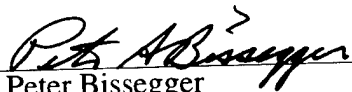
Engineering and Technology Group

19990316 005

This report was submitted by The Aerospace Corporation, El Segundo, CA 90245-4691, under Contract No. F04701-93-C-0094 with the Space and Missile Systems Center, 2430 E. El Segundo Blvd., Los Angeles Air Force Base, CA 90245. It was reviewed and approved for The Aerospace Corporation by A. B. Christensen, Principal Director, Space and Environment Technology Center. Peter Bissegger was the project officer for the Mission-Oriented Investigation and Experimentation (MOIE) program.

This report has been reviewed by the Public Affairs Office (PAS) and is releasable to the National Technical Information Service (NTIS). At NTIS, it will be available to the general public, including foreign nationals.

This technical report has been reviewed and is approved for publication. Publication of this report does not constitute Air Force approval of the report's findings or conclusions. It is published only for the exchange and stimulation of ideas.

A handwritten signature in dark ink, appearing to read "Peter Bissegger", is written over a horizontal line.

Peter Bissegger
SMC/AXES

REPORT DOCUMENTATION PAGEForm Approved
OMB No. 0704-0188

Public reporting burden for this collection of information is estimated to average 1 hour per response, including the time for reviewing instructions, searching existing data sources, gathering and maintaining the data needed, and completing and reviewing the collection of information. Send comments regarding this burden estimate or any other aspect of this collection of information, including suggestions for reducing this burden to Washington Headquarters Services, Directorate for Information Operations and Reports, 1215 Jefferson Davis Highway, Suite 1204, Arlington, VA 22202-4302, and to the Office of Management and Budget, Paperwork Reduction Project (0704-0188), Washington, DC 20503.

1. AGENCY USE ONLY (Leave blank)		2. REPORT DATE 20 December 1998	3. REPORT TYPE AND DATES COVERED	
4. TITLE AND SUBTITLE High-Speed Ion Flow, Substorm Current Wedge, and Multiple Pi 2 Pulsations			5. FUNDING NUMBERS F04701-93-C-0094	
6. AUTHOR(S) K. Shiokawa, W. Baumjohann, G. Haerendel, G. Paschmann, J. F. Fennell, E. Friis-Christensen, H. Lühr, G. D. Reeves, C. T. Russell, P. R. Sutcliffe, and K. Takahashi				
7. PERFORMING ORGANIZATION NAME(S) AND ADDRESS(ES) The Aerospace Corporation Technology Operations El Segundo, CA 90245-4691			8. PERFORMING ORGANIZATION REPORT NUMBER TR-99(8570)-3	
9. SPONSORING/MONITORING AGENCY NAME(S) AND ADDRESS(ES) Space and Missile Systems Center Air Force Materiel Command 2430 E. El Segundo Boulevard Los Angeles Air Force Base, CA 90245			10. SPONSORING/MONITORING AGENCY REPORT NUMBER SMC-TR-99-04	
11. SUPPLEMENTARY NOTES				
12a. DISTRIBUTION/AVAILABILITY STATEMENT Approved for public release; distribution unlimited			12b. DISTRIBUTION CODE	
13. ABSTRACT (Maximum 200 words) We have studied the onset timing of earthward high-speed ion flow observed by the AMPTE/IRM satellite at 12.3 Earth radii (R_E) and 0100 MLT in the central plasma sheet during an isolated substorm event on March 1, 1985. The timing of this onset is compared with that of the substorm current wedge and Pi 2 magnetic pulsations observed by a large number of ground-based stations and the AMPTE/CCE, GOES 5, and ISEE 1 satellites and with that of high-energy particle injection observed at Los Alamos geosynchronous satellite 1982-019. The onset of earthward high-speed flow is observed 3 min before the onset of the global current wedge formation and 6 min before the onset of high-energy particle injection. The three bursts of the high-speed flow observed at AMPTE/IRM are likely to correspond to three compressional pulses observed at AMPTE/CCE at 6 R_E and three Pi 2 wave packets observed at midlatitude ground stations. On the basis of these observations, we conclude that the substorm current wedge is caused by inertia current and the current due to flow shear at the braking point of the earthward high-speed flow during the initial stage of the substorm expansion phase. The braking point is well separated from the near-Earth neutral line. It is also suggested that the compressional pulses and fluctuations of field-aligned currents generated at the flow braking point can be the initial cause of the Pi 2 magnetic pulsations in the inner magnetosphere.				
14. SUBJECT TERMS Substorms, Current wedge, Plasma sheet, Ions, Plasma flow			15. NUMBER OF PAGES 17	
			16. PRICE CODE	
17. SECURITY CLASSIFICATION OF REPORT UNCLASSIFIED	18. SECURITY CLASSIFICATION OF THIS PAGE UNCLASSIFIED	19. SECURITY CLASSIFICATION OF ABSTRACT UNCLASSIFIED	20. LIMITATION OF ABSTRACT	

Acknowledgments

We are grateful to N. Sckopke for his help in accessing the AMPTE/IRM particle distribution functions. K. S. is also grateful to T. M. Bauer and M. Scholer for fruitful discussions. We would like to thank G. Jansen van Beek and the Geological Survey of Canada for providing 1 min and 10-s sampled magnetic field data from their Canadian stations. The 10-s data at Ottawa and 1 min data at St. John's are crucially important to the present study. We also would like to thank T. Iyemori of WDC-C2 for Geomagnetism at Kyoto University for providing us with the 1 min sampled magnetic field data at 13 stations, 1-s sampled magnetic field data at Kakioka, and the AU and AL indices. The magnetic field data from the observatories in Iceland were provided by the Upper Atmosphere Physics Group at the National Institute of Polar Research, Japan. The EISCAT magnetometer data used here (KIL) were collected as a German-Finnish cooperation conducted by the Technical University of Braunschweig and the Finnish Meteorological Institute Helsinki. The 3-s sampled GOES 5 magnetic field data were provided by WDC-A at National Geophysical Data Center. The routine to convert the GOES data from PEN coordinates to HVD coordinates was provided by T. Nagai. The magnetic field line tracing and coordinate transformation were done using T89c and GEOPACK routines provided by N. A. Tsyganenko and NASA/GSFC Magnetospheric Modeling Group. The calculation of magnetic latitudes and local times was done by routines written by N. Nishitani, while the routines to make PostScript plots were provided by T. Ogino and K. Ota, all at the Solar-Terrestrial Environment Laboratory, Nagoya University. The work at UCLA was supported by the National Science Foundation under research grant ATM 94-13081. K. S. is supported by the Ministry of Education, Science, and Culture of Japan with a Grant-in-Aid for Overseas Research Scholar (8-Wakate-70).

Contents

1.	Introduction.....	1
2.	Data Sets Used	2
3.	AMPTE/IRM Observations in the Tail.....	3
4.	Ground-Based Signatures of Substorm Currents	6
5.	Ground-Based Signatures of Pi 2 Pulsations	8
6.	Magnetic Observations Around the Geosynchronous Orbit.....	9
7.	Summary and Discussion	10
	7.1 Relation of High-Speed Flow, Current Wedge, and Particle Injection.....	13
	7.2 Relation Between High-Speed Ion Flow and Pi 2 Pulsations.....	15
8.	Conclusions.....	16
	References	16

Figures

1.	AU and AL indices on March 1, 1985	2
2.	GSM-XY and GSM-XZ plane projections of the satellites available for use in this study at 0240 UT on March 1, 1985	2
3.	Magnetic latitude (MLAT) and MLT of the ground-based stations and footprints of satellites used in the present study	3
4.	Plasma moments and magnetic field data in GSM coordinates measured on board the AMPTE/IRM satellite at 5-s resolution	4
	Plate 1.....	5
5.	H (positive, northward) and D (positive, eastward) component magnetic field traces from high-latitude stations at 10-s resolution at Isafjordur (ISA) and Tjornes (TJR) and at 1 min resolution at other stations.....	6

6. H (positive, northward) and D (positive, eastward) component magnetic field traces from midlatitude stations at 10-s resolution at Ottawa (OTT) and Victoria (VIC) and at 1 min resolution at other stations in the same format as that in Figure 5	7
7. H and Z component magnetic field traces from NAQ and Sanae (SNA) at 1 min resolution	8
8. H and D component magnetic field fluctuations observed at midlatitude stations at Kakioka (KAK), HER, OTT, and VIC.....	8
9. Hodograms of the four successive Pi 2 pulsations observed at OTT in the premidnight sector (2100 MLT) and at HER in the postmidnight sector (0300 MLT)	9
10. Magnetic field data measured on the AMPTE/CCE satellite in the D, F, and A coordinates	9
11. Magnetic field data measured on the GOES 5 satellite in the V, D, and H coordinates....	10
12. Magnetic field data measured on the ISEE 1 satellite in the GSE coordinates.....	11
13. Comparison of the onset timings of high-speed ion flow in the near-Earth tail, ground signatures of westward electrojet and substorm current wedge, and particle injections at geosynchronous orbit, in the midnight sector	12
14. Comparison of the high-speed ion flow in the near-Earth tail, westward electrojet in the auroral zone, and Pi 2 magnetic pulsations and compressional pulses observed at ground stations and satellites in the inner magnetosphere.....	12
15. Proposed model of the current wedge formation during the initial stage of the substorm expansion phase.....	14

1. Introduction

Earthward high-speed ion flow in the near-Earth central plasma sheet has been studied extensively in recent years using plasma data from the Active Magnetospheric Particle Tracer Explorer/Ion Release Module (AMPTE/IRM) satellite [e.g., Baumjohann *et al.*, 1990; Angelopoulos, 1996, and references therein]. The flow is bursty with a duration of only a few minutes [Angelopoulos *et al.*, 1992, 1994a]. The positive correlation between the *AE* index and the occurrence of the high-speed flow [Baumjohann *et al.*, 1990] and several multipoint studies of the flow events [e.g., Lopez *et al.*, 1994; Sergeev *et al.*, 1995; Angelopoulos *et al.*, 1996] indicate that the high-speed flow occurs during magnetospheric substorms. In fact, Russell and McPherron [1973] have included an inward moving plasma flow deduced from the magnetic field compressions observed by radially aligned ATS 1 and OGO 5 satellites as a feature of the original near-Earth neutral point model of substorms.

The onset of a substorm expansion phase is accompanied by the sudden decrease in tail current intensity (tail current disruption) [e.g., Fairfield and Ness, 1970] and the formation of a pair of downward (on the dawnside) and upward (on the duskside) field-aligned currents (substorm current wedge) [e.g., Akasofu, 1972; McPherron *et al.*, 1973]. There is an apparent discrepancy between the region of what has been called the "tail current disruption" and the source of the high-speed flow. That is, the current disruption determined from in situ magnetic field observations by satellites usually starts in the near-Earth magnetotail often within $15 R_E$ of the Earth [e.g., Ohtani *et al.*, 1988; Jacquey *et al.*, 1991], while the high-speed flow is mostly earthward at $|X| < 20 R_E$, indicating that the source of the flow is tailward of this distance [e.g., Baumjohann *et al.*, 1990].

Several models of substorm expansion onset that give explanations of this discrepancy have been proposed [see, e.g., McPherron, 1995]. Lui [1991a] and Ohtani *et al.* [1992] explained this discrepancy by tailward expansion of the region of current disruption and/or of rarefaction waves in which earthward flow is generated on the basis of the current disruption model. Baker and McPherron [1990] and Baker *et al.* [1993] suggested that this discrepancy is caused by the slow reconnection process on closed field lines during the substorm growth phase on the basis of the near-Earth neutral line model.

On the other hand, a few authors have focused on the braking processes of the earthward high-speed flow in the near-Earth tail as the cause of the current disruption.

The braking processes generate dawnward (eastward) inertia current [Haerendel, 1992], pileup of northward magnetic flux [Hesse and Birn, 1991], and field-aligned current due to flow shear [Hasegawa, 1979]. These processes can account for the discrepancy between the region of current disruption and the source of the flows. Shiokawa *et al.* [1997] concluded that the braking point of the flow is the boundary between dipolar and tail-like magnetic field configurations at the inner edge of the neutral sheet.

The onset of a substorm expansion phase is also accompanied by a damped magnetic pulsation termed Pi 2 [e.g., Saito, 1969; Yumoto, 1986]. All Pi 2 models assume an initial driving force which comes from the tail to the inner magnetosphere associated with the current wedge formation [e.g., Yeoman and Orr, 1989]. The braking of high-speed ion flow in the central plasma sheet may give the initial impulse.

In the present analysis we have investigated the onset timing of high-speed ion flow, current wedge, and multiple Pi 2 pulsations for an isolated substorm on March 1, 1985, using a number of data points in space and on the ground. Though there have been many case studies of substorms using multi-instruments, few studies have focused on the onset timing using the earthward high-speed flow data in the central plasma sheet. The observed signatures of these substorm indicators are fairly consistent with the idea that the braking point of the high-speed flow has a crucial importance in the current wedge formation during the initial stage of the substorm expansion phase.

2. Data Sets Used

Figure 1 shows the *AU* and *AL* indices during the substorm event on March 1, 1985. We focus our analysis mainly on the interval 0220–0320 UT. A small substorm takes place around 0240 UT, reaching a maximum *AE* index of 395 nT at 0251 UT.

Figure 2 shows GSM-XY and GSM-XZ plane orbit projections at 0240 UT on March 1, 1985 for the satellites used in this study. We used 5-s resolution data from the magnetic field instrument [Lühr *et al.*, 1985] and the three-dimensional (3-D) plasma analyzer [Paschmann *et al.*, 1985] on board the AMPTE/IRM satellite at a GSM position $(-11.8, -2.6, -2.2) R_E$. Data from two geosynchronous satellites are available, with 1 min resolution energetic particle data measured on board the Los Alamos National Laboratory (LANL) 1982-019 satellite located at $(-6.6, 0.3, -0.9) R_E$ and magnetic field data at 3-s resolution from the GOES 5

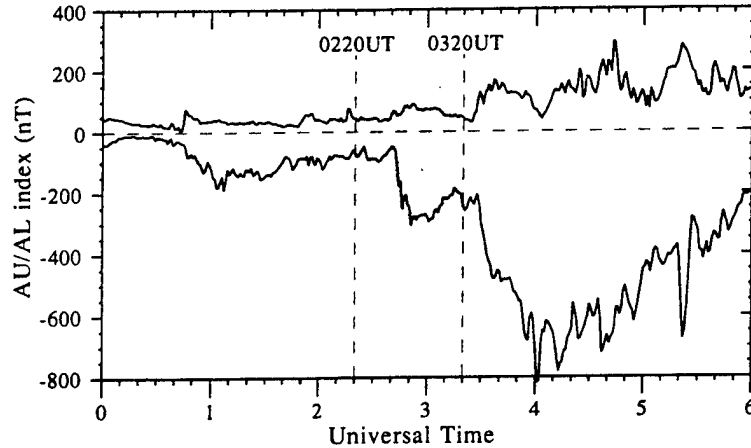


Figure 1. AU and AL indices on March 1, 1985. The data analyses in this paper are mostly focused on the interval of 0220–0320 UT which is shown as the shaded area.

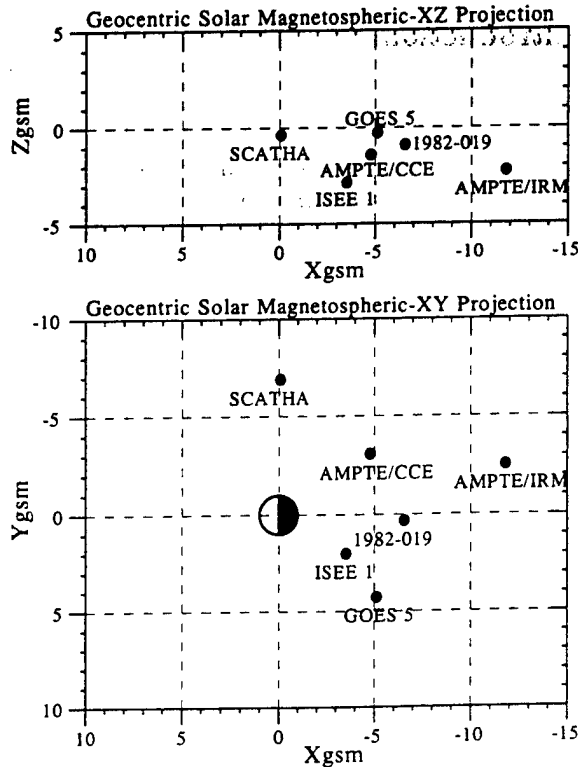


Figure 2. GSM-XY and GSM-XZ plane projections of the satellites available for use in this study at 0240 UT on March 1, 1985.

spacecraft located at $(-5.1, 4.2, -0.2) R_E$. Three other spacecraft are also near the synchronous orbit. The data used are spin-averaged magnetometer data at ~ 6 -s resolution [Potemra *et al.*, 1985] from the AMPTE/CCE satellite at $(-4.8, -3.1, -1.4) R_E$, magnetic field data at 0.25-s resolution measured by the SCATHA spacecraft at $(-0.1, -6.9, -0.3) R_E$, and magnetic field data at 4-s resolution from the University of California, Los Angeles (UCLA), fluxgate magnetometer [Russell, 1978] on board the ISEE 1 satellite at $(-3.6, 1.9, -2.8) R_E$. ISEE 1 is located at latitudes higher than other satellites.

Figure 3 shows the magnetic latitude (MLAT) and MLT of the satellite footprints. The field line tracing from the satellite altitudes to an altitude of 100 km is performed using the T89 model [Tsyganenko, 1989] for $K_p = 2$. All the footprints are between 63° and 67° MLAT and distributed from 2100 to 0600 MLT through midnight. The footprints of AMPTE/IRM and 1982-019 are located fairly close to midnight.

In addition to the satellite data, we used magnetic field data measured at 48 ground-based stations. Data from 21 stations shown in Figure 3 and data from Kakioka (KAK, Japan, not shown in Figure 3) will be presented in this paper. Data at 1-s resolution are available at Hermanus (HER, South Africa), two Iceland stations at Isafjordur (ISA) and Tjornes (TJR), and at Kakioka. Data at 10-s resolution are available at Victoria (VIC, Canada) and Ottawa (OTT, Canada). It is possible to check Pi 2 magnetic pulsations using these high-resolution data at midlatitude stations. Data from other stations are at 1 min resolution. A dense magnetometer network is available in Greenland, which is very close to the footprint of AMPTE/IRM in the midnight sector.

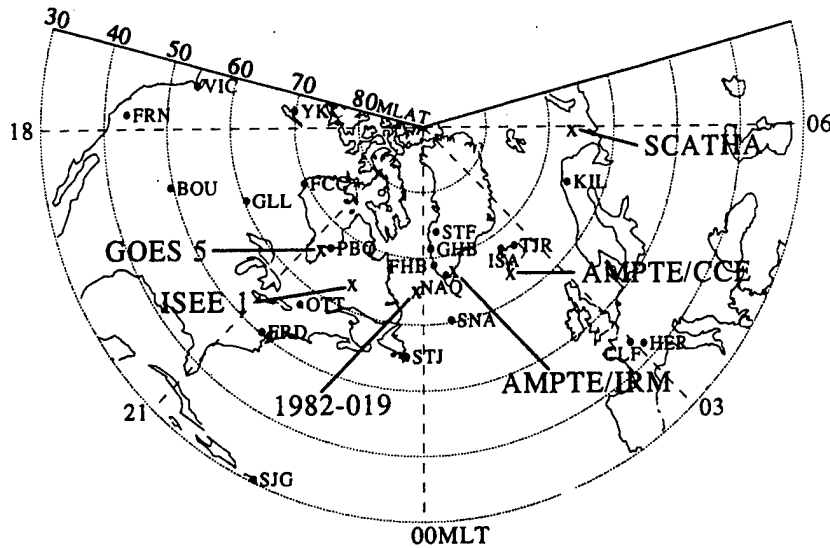


Figure 3. Magnetic latitude (MLAT) and MLT of the ground-based stations and footprints of satellites used in the present study. The field line tracing from the satellite altitudes to an altitude of 100 km in the northern hemisphere was done using T89 model [Tsyganenko, 1989] for $Kp = 2$. The points shown as HER (Hermanus, South Africa) and SNA (Sanac, Antarctica) are the magnetic conjugate points in the northern hemisphere.

3. AMPTE/IRM Observations in the Tail

Figure 4 shows plasma moments and magnetic field data from AMPTE/IRM for 0220–0320 UT. AMPTE/IRM is in the near-Earth tail at $\sim 12 R_E$ in the midnight sector (0100 MLT). The vertical distance Z_{ns} from the model neutral sheet by Fairfield [1980] is less than $1 R_E$. During the interval shown, AMPTE/IRM is mostly in the inner central plasma sheet as defined by Baumjohann *et al.* [1989].

For 0220–0237 UT, no flow is seen in any component in Figures 4c, 4d, and 4e. Weak duskward flow starts around 0237 UT. Then, an intense earthward ion flow is observed after 0238 UT with a maximum flow velocity of more than 1000 km s^{-1} . The flow turns weakly tailward at 0243 UT, and then it turns back and forth until ~ 0256 UT.

The magnetic field intensity in Figure 4i increases continuously before the flow onset, between 0231–0237 UT. The increase stops at 0237 UT when the duskward flow starts. During the high-speed flow, for 0239–0247 UT, the field intensity strongly fluctuates. The amplitude of the fluctuation is almost comparable to the average intensity.

To see temporal change of the particle spectra, we show energy- and angle-time spectrograms obtained by

AMPTE/IRM for 0210–0310 UT in Plate 1 with the elevation and azimuth angles of the magnetic field vector. The 3-D distribution functions of ions in this event were shown by Nakamura *et al.* [1991] and further discussed by Speiser and Martin [1996].

Before the onset of the high-speed flow the ion and electron energy gradually decreases for 0210–0238 UT as shown in Plate 1 (top and fourth spectrograms), respectively. This corresponds to the decrease of ion temperature shown in Figure 4a. The elevation angle of the magnetic field continuously decreases toward the tail-like field as shown in the bottom panel of Plate 1.

Then, the ion energy suddenly increases to more than 10 keV at 0239 UT, and high-speed earthward flow is observed at small elevation and azimuth angles (Plate 1, second and third spectrograms). The electrons are almost isotropic during the high-speed flow. Note that the elevation angle of the magnetic field remains small (tail-like) during the high-speed flow until 0242 UT but becomes dipolar when the flow turns tailward at 0243 UT.

Intense counterstreaming electrons parallel and antiparallel to the magnetic field line are observed from 0247 UT, when the magnetic field becomes dipolar and

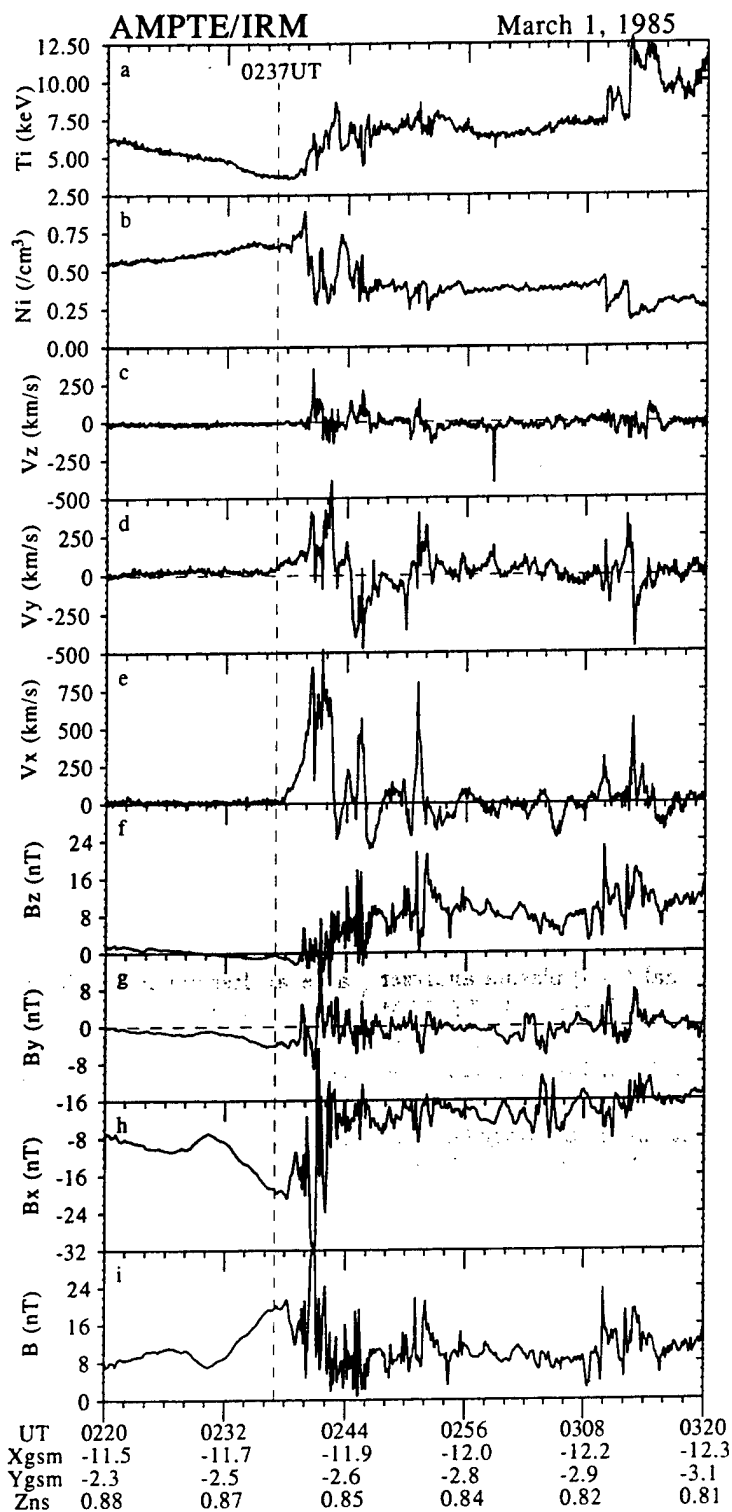


Figure 4. Plasma moments and magnetic field data in GSM coordinates measured on board the AMPTE/IRM satellite at 5-s resolution. V_x , V_y , and V_z correspond to the ion bulk velocities in X , Y , and Z directions, respectively. Satellite locations in units of Earth radii are shown at the bottom of these panels in GSM- XY coordinates, while Z_{ns} is the vertical distance from the model neutral sheet by Fairfield [1980]. The vertical dashed line at 0237 UT indicates the onset time of ion flow.

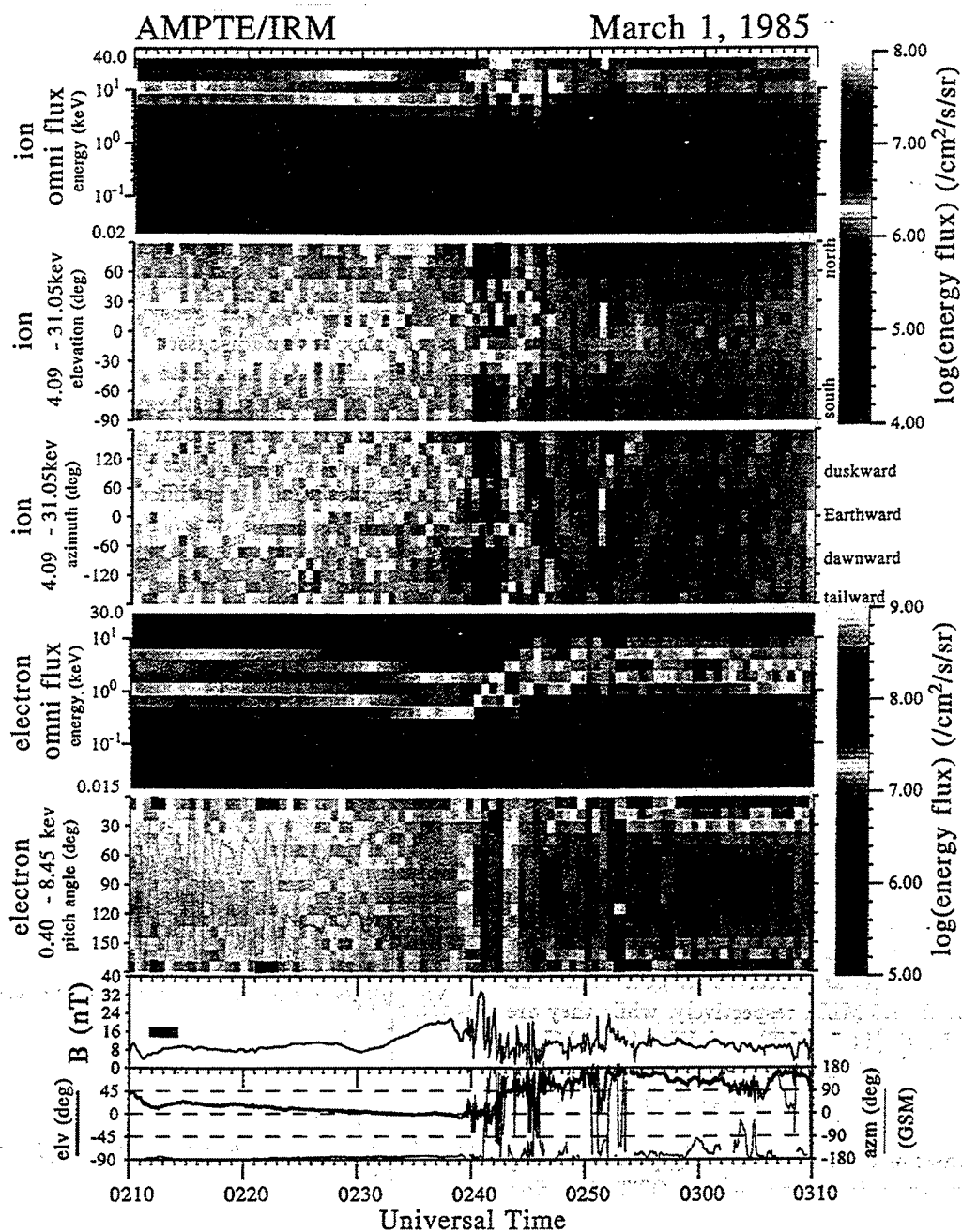


Plate 1. From top to bottom: energy-time spectra of omni-directional ions, elevation-time spectra, and azimuth-time spectra of ions in GSM coordinates for energies of 4.09–31.05 keV, energy-time spectra of omni-directional electrons, pitch angle-time spectra of electrons for energies of 0.4–8.45 keV, magnetic field intensity, and elevation (thick line) and azimuth (thin line) of the magnetic field in GSM coordinates measured on board the AMPTE/IRM satellite for 0210–0310 UT. The particle spectra are at 39-s resolution, while the magnetic field data are at 5-s resolution.

the high-speed ion flow stops. Note that the counterstreaming electrons do not coincide with the high-speed ion flow even after this time. For example, when the ion flow burst appears at 0251 UT, the counterstreaming electrons disappear.

4. Ground-Based Signatures of Substorm Currents

Figure 5 shows magnetic field variations at auroral zone stations during this event. A clear onset of westward electrojet current (sudden decrease in H component) is first observed at Narsarsuaq (NAQ, Greenland) at 0241 UT in the midnight sector (0.6 MLT). The decrease of H at NAQ between 0241 and 0242 UT

amounted to 30 nT. Note that NAQ is close to the footprint of AMPTE/IRM as shown in Figure 3. The onset of the H and D variations at FHB (Frederikshab), which is 1.7° poleward and 0.3 hours westward of NAQ, is clearly ~ 5 min later than those at NAQ, indicating that the onset region of the westward electrojet is quite localized.

Figure 6 shows magnetic field variations at stations in midlatitudes and subauroral latitudes. A clear onset of a positive H bay is observed at St. John's (STJ) at 0241 UT in the midnight sector (23.7 MLT). At this time, the H component starts to decrease at stations in the premidnight sector (e.g., at OTT, Gillam (GLL), and Boulder (BOU)), while no clear H variations are seen at stations in the postmidnight sector. The time 0241 UT corresponds to the onset time of H decrease at NAQ in Figure 5.

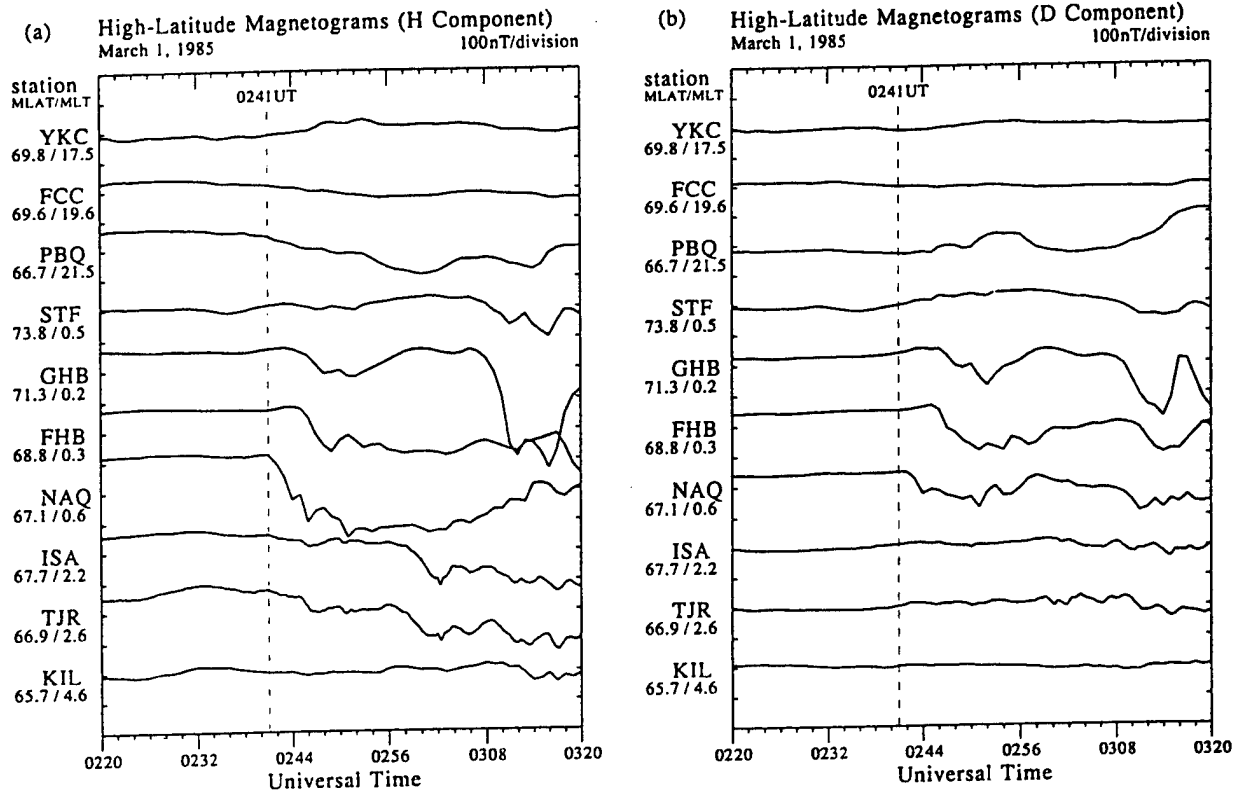


Figure 5. (a) H (positive, northward) and (b) D (positive, eastward) component magnetic field traces from high-latitude stations at 10-s resolution at Isafjordur (ISA) and Tjornes (TJR) and at 1 min resolution at other stations. From top to bottom, stations are distributed from evening to morning sectors through midnight. MLAT and MLT of each station at 0240 UT are shown in the left side of these panels. The vertical dashed line at 0241 UT indicates the onset time of westward electrojet currents which is identified from the negative H decrease at Narsarsuaq (NAQ, Greenland) in the midnight sector.

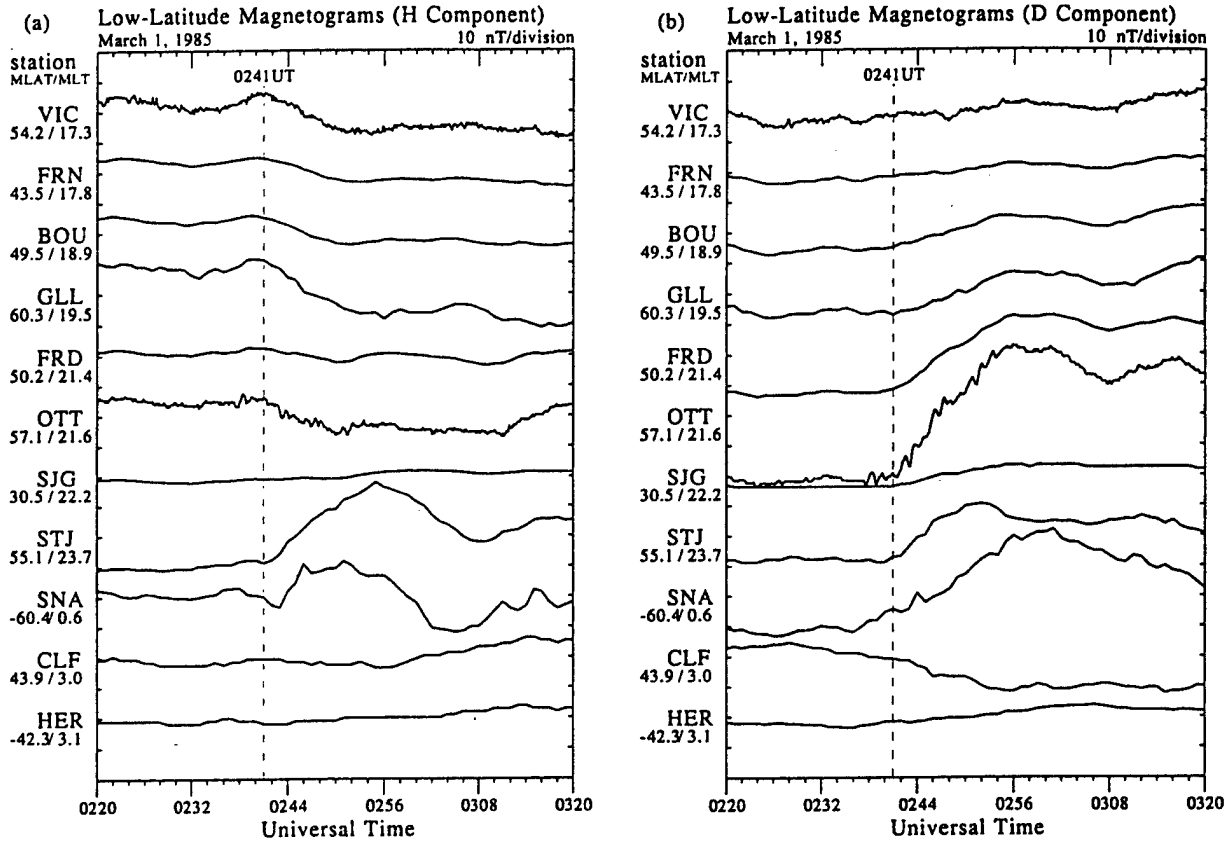


Figure 6. (a) H (positive, northward) and (b) D (positive, eastward) component magnetic field traces from midlatitude stations at 10-s resolution at Ottawa (OTT) and Victoria (VIC) and at 1 min resolution at other stations in the same format as that in Figure 5. From top to bottom, stations are distributed from evening to morning sectors through midnight. The vertical dashed line at 0241 UT indicates the onset time of positive H bay at St. John's (STJ) in the midnight sector. The time also corresponds to the onset of D enhancement at OTT in the premidnight sector.

The time 0241 UT also corresponds to the onset time of positive D enhancement at STJ in the midnight sector and at OTT in the premidnight sector (21.6 MLT). This D enhancement suggests that the center of the current wedge is located eastward of STJ. Such D enhancement is small at San Juan (SJG), probably because SJG is located at a lower latitude than the others.

NAQ is the southmost station in Greenland as shown in Figure 3. To check the possibility that the first onset of westward electrojet current occurs equatorward of NAQ, we plotted Z component magnetic field variations at NAQ and Sanae (SNA, Antarctica) in Figure 7. Before the H decrease at NAQ (0241 UT), the Z components start to increase (downward) at NAQ. This Z variation clearly indicates that westward electrojet current is formed equatorward of NAQ at 0237 UT.

The only low-latitude signatures which correspond to the onset of the Z increase at NAQ (Figure 7) are the eastward enhancement of D (Figure 6) and the downward enhancement of Z (Figure 7) at SNA at 0237 UT. The Z variation is probably caused by the field-aligned currents of the current wedge, while the D variation may suggest that the current wedge is formed westward of SNA (0.6 MLT) at this time. It should be noted, however, that the magnetic field variations at SNA may be affected by westward electrojet current rather than the field-aligned current since a clear positive H bay is not seen around 0237 UT at SNA as shown in Figure 6.

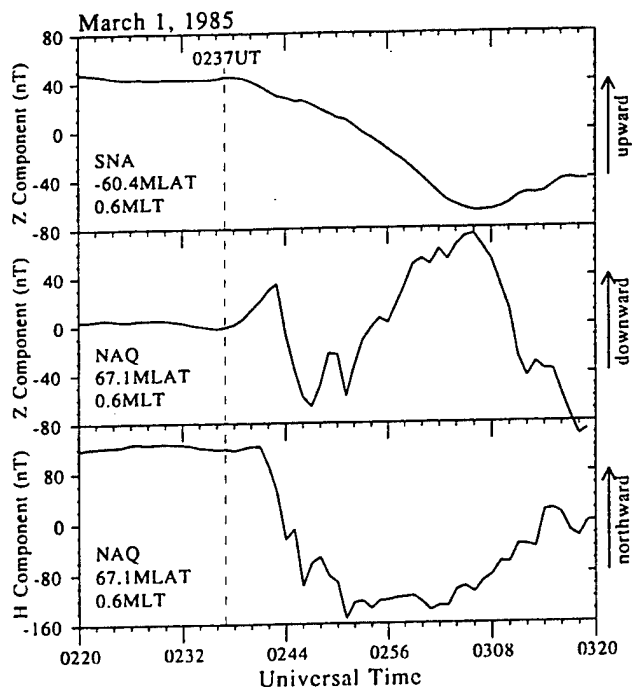


Figure 7. H and Z component magnetic field traces from NAQ and Sanae (SNA) at 1 min resolution. MLAT and MLT of each station at 0240 UT are shown. The vertical dashed line at 0237 UT indicates the onset time of westward electrojet current which is identified from the Z variations.

5. Ground-Based Signatures of Pi 2 Pulsations

In the 10-s-sampled D component data at OTT in Figure 6, several wave packets of Pi 2 magnetic pulsation are seen around the onset of the substorm. To see these Pi 2 features more clearly, we present in Figure 8 filtered magnetograms from stations where high time resolution data are available.

The Pi 2 pulsations are observed at both HER and OTT at 3.1 and 21.6 MLT, respectively, while they are not clear at KAK (11.7 MLT) and VIC (17.3 MLT). Four wave packets of Pi 2 pulsations can be identified in the data at OTT with onset times at 0237, 0241, 0245, and 0250 UT. The second Pi 2 at 0241 UT is accompanied by the onset of H decrease at NAQ, positive H bay at STJ, and positive D enhancement at OTT. The first Pi 2 onset at 0237 UT is accompanied by the onset of Z increase at NAQ. Note that the onset time of the first Pi 2 pulsation is slightly earlier at HER (at 0236:30 UT in the D component) than at OTT (at 0237:00 UT).

Polarization patterns of Pi 2 pulsations indicate the locations of Pi 2 current system [Lester *et al.*, 1983, 1984]. We plot the hodogram of the four Pi 2 wave packets in Figure 9. The directions of the major axes of the Pi 2 polarization at OTT are always eastward for all the Pi 2 wave packets. The second, the third, and the fourth hodogram at OTT are closer to circular polarization than the first one. The directions at HER, converted to the northern hemisphere, are eastward for the first Pi 2, while they are westward for the other three Pi 2 wave packets. For the simple model of substorm current wedge [see Lester *et al.*, 1984, Figure 1], the center of the Pi 2 current system is probably between OTT (21.6 MLT at 0240 UT) and HER (3.1 MLT) for

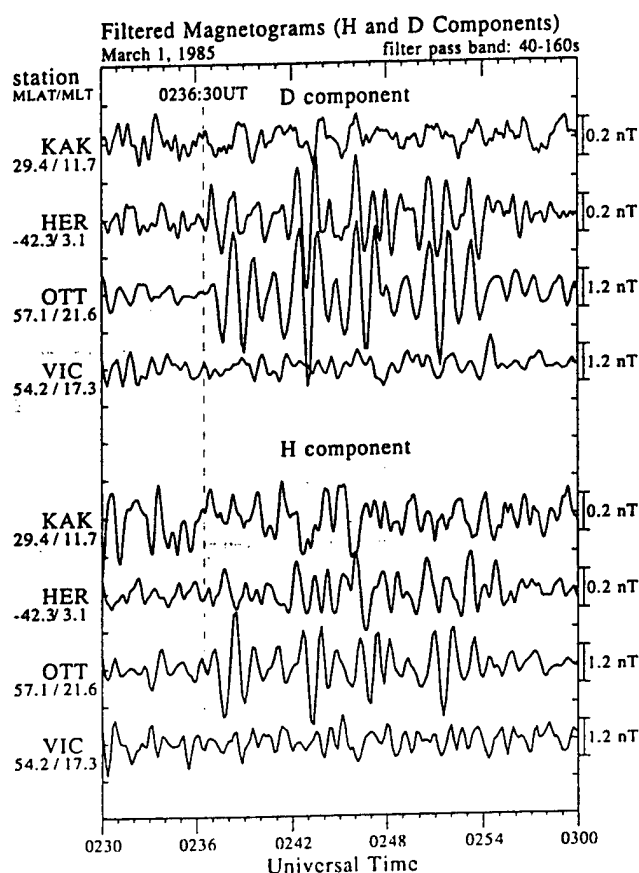


Figure 8. H and D component magnetic field fluctuations observed at midlatitude stations at Kakioka (KAK), HER, OTT, and VIC. MLAT and MLT of each station at 0240 UT are shown in the left side of these panels. Data at KAK and HER are at 1-s resolution, while those at OTT and VIC are at 10-s resolution. A band-pass filter with a period range of 40–160 s is used. The vertical dashed line at 0236:30 UT indicates the onset time of the first Pi 2 pulsation in the D component at HER.

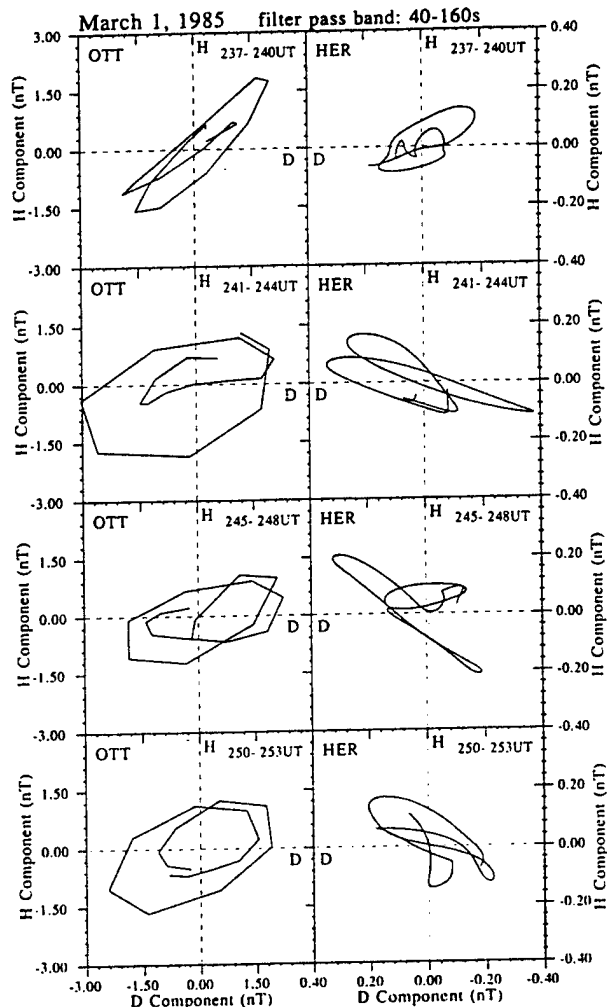


Figure 9. Hodograms of the four successive Pi 2 pulsations observed at OTT in the premidnight sector (2100 MLT) and at HER in the postmidnight sector (0300 MLT). The D component fluctuations at HER are plotted in opposite direction (positive, left side) to show the polarization azimuths expected in the northern hemisphere. A band-pass filter with a period range of 40–160 s is used.

all four Pi 2 pulsations. The center for the first Pi 2 is likely to be westward from the center of the second to fourth Pi 2.

6. Magnetic Observations Around the Geosynchronous Orbit

In this section we show magnetic field data from four satellites (AMPTE/CCE, GOES 5, and ISEE 1), which are located near geosynchronous orbit during

the substorm event discussed in this paper. Figure 10 shows magnetic field data measured on board the AMPTE/CCE satellite in the postmidnight sector (2.1 MLT at 0240 UT). The total magnetic field intensity decreases continuously in this plot since AMPTE/CCE is leaving the Earth. It is difficult to define a clear substorm onset from this data. However, there are three clear pulses in the northward and total components of the magnetic field data with peaks at 0242, 0246, and

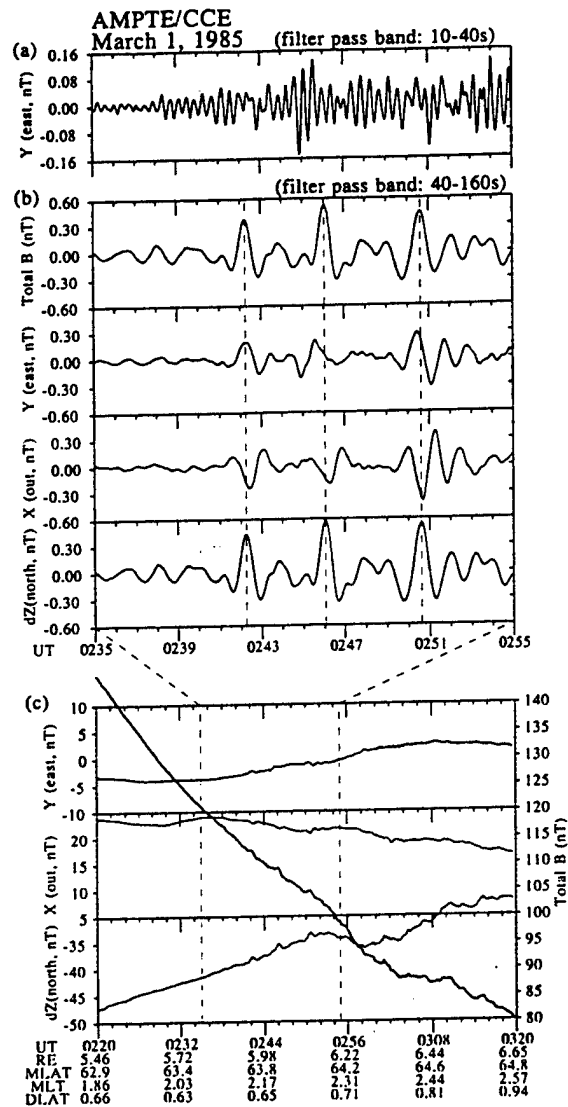


Figure 10. Magnetic field data measured on the AMPTE/CCE satellite in the D , F , and A coordinates, where the Z axis is along the field line of the dipole field derived from a simple Earth-centered dipole moment, Y is magnetically eastward, and X is radially outward.

The value dZ is the perturbation relative to the model field strength. Because the satellite was very close to the magnetic equator, the D , F , and A coordinates and the more familiar V , D , and H coordinates are almost equivalent. Total magnetic field intensity in Figure 10c (thick line) continuously decreases because the satellite is leaving the Earth. UT and satellite locations are shown at the bottom of the panels, where RE, MLAT, MLT, and DLAT are distance from the Earth center in unit of Earth radii, magnetic latitude, magnetic local time, and dipolar geomagnetic latitude of the satellite, respectively. A band-pass filter with a period range of 40–160 s is used to show the magnetic field variations in Figure 10b, while that with a period range of 10–40 s is used to show the magnetic field variations in Figure 10a. The three vertical lines in Figure 10b indicate the peaks of the compressional pulses seen in the total component.

0250 UT as shown by the dashed lines in Figure 10b. The three pulses also correspond to decreases of the outward component, indicating that the pulses turn the field into a more dipolar configuration. It is noted, however, that they are mainly compressional pulses seen in the total component.

As shown in Figure 10a, weak magnetic field oscillation with periods of 10–40 s is observed after 0238 UT mainly in the Y (east-west) component. Though AMPTE/CCE is quite close to the magnetic equator, this oscillation may be categorized as transient toroidal waves which have been discussed by *Takahashi et al.* [1996].

Figure 11 shows magnetic field data measured on board the GOES 5 satellite in the premidnight sector (21.3 MLT at 0240 UT). The northward and total components decrease from around 0242 to 0252 UT and then increase after 0252 UT. The eastward component increases from 0236 to 0252 UT and then decreases until about 0310 UT. These variations of magnetic fields are consistent with the typical magnetic field changes seen in the evening sector during substorms [e.g., *Nagai*, 1991]. However, it is difficult to define a substorm onset time from this data. Intense magnetic field oscillations with a period of ~ 2 min are seen in all components with an onset time at about 0242 UT. The period is slightly longer than that of the Pi 2 pulsations simultaneously observed at ground-based stations.

The ISEE 1 satellite is also located in the premidnight sector (22.3 MLT at 0240 UT) but off the equatorial plane, at dipolar latitudes of $\sim 20^\circ$. The magnetic field data on board the ISEE 1 satellite are shown in

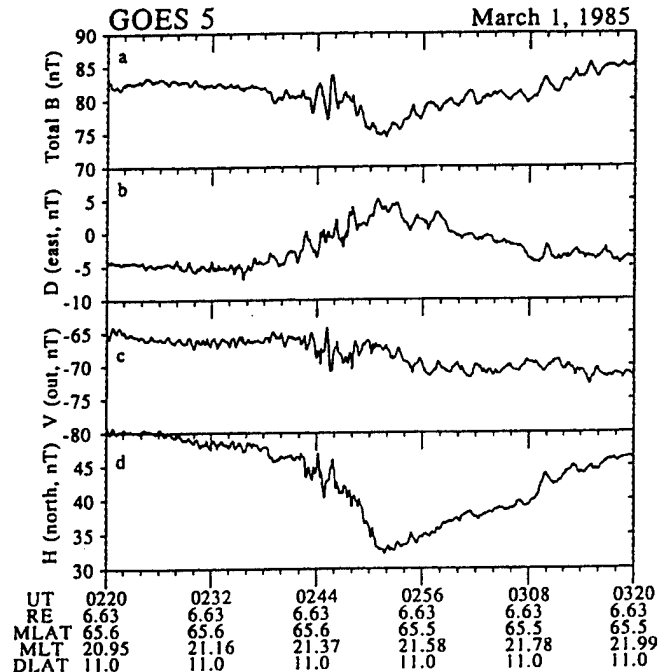


Figure 11. Magnetic field data measured on the GOES 5 satellite in the V , D , and H coordinates, where H is along the dipole axis (northward, positive), D is azimuthally eastward, and V is radially outward. Universal time (UT) and satellite locations are shown at the bottom in the same format as that in Figure 10.

Figure 12. Magnetic field oscillations with a period of ~ 2 min are seen in the GSE- X and GSE- Y components and weakly in the total component. The oscillations are mainly in the component perpendicular to the ambient magnetic field. Probably, they are again categorized as transient toroidal waves. The onset time of the oscillations is ~ 0237 UT.

The SCATHA satellite was in the morning sector (5.9 MLT at 0240 UT) during the event (data are not shown in this paper). No significant DC magnetic field change was observed by SCATHA, while magnetic pulsations could not be identified because of the intense artificial spin modulations in the data.

7. Summary and Discussion

For the substorm event discussed in this paper the onset of high-speed earthward ion flow is observed by AMPTE/IRM (section 3). The formation of the substorm current system can be also identified from the dense network of ground-based magnetometers (section 4). Four Pi 2 wave packets are identified from ground-

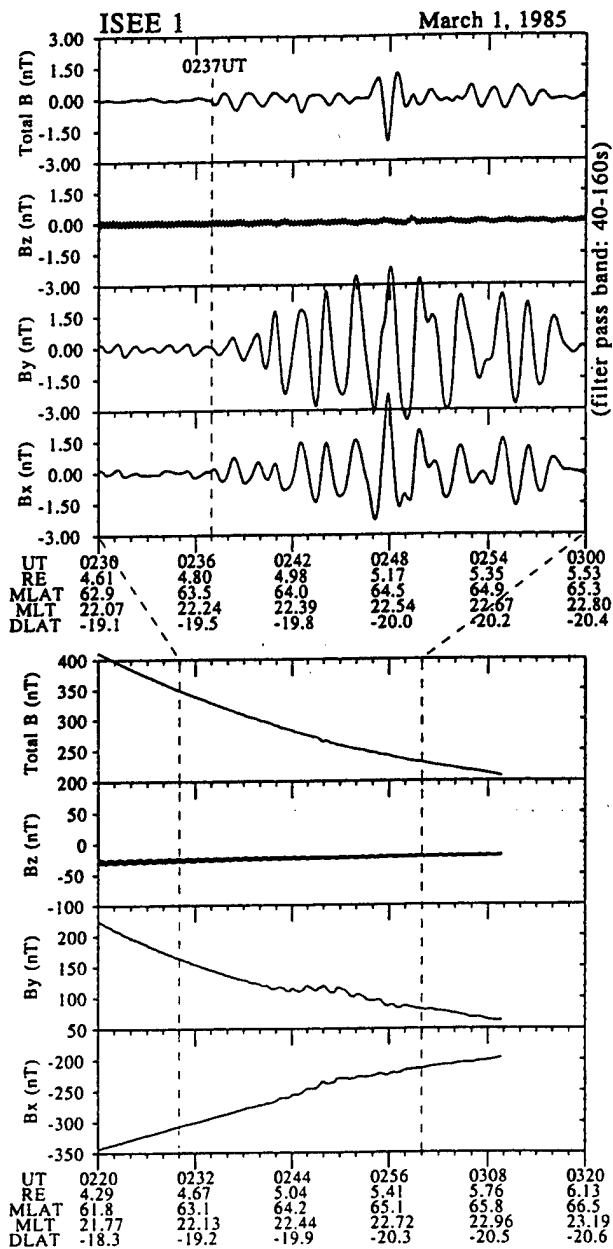


Figure 12. Magnetic field data measured on the ISEE 1 satellite in the GSE coordinates. UT and satellite locations are shown at the bottom of these panels in the same format as that in Figure 10. A band-pass filter with a period range of 40–160 s is used to show the magnetic field variations in Figure 12a. The vertical dashed line at 0237 UT in Figure 12a indicates the onset time of the magnetic pulsations in the total component.

based observations (section 5). Compressions and oscillations of magnetic field are observed by satellites around geosynchronous orbit (section 6).

In Figure 13 we compare the observed onset time of high-speed ion flow and the formation of the substorm current system. The high-energy particle data obtained by the geosynchronous satellite 1982-019 in the midnight sector (23.9 MLT at 0240 UT) are also shown at the bottom. The onset of ion flow is around 0237 UT in the V_y component at AMPTE/IRM. This time is nearly equal to the onset time of the first Pi 2 pulsation at HER at 0236:30 UT shown by the leftmost vertical dashed line. The onsets of negative H bay at NAQ, positive H bay at STJ, and positive D enhancement at OTT are all at 0241 UT (second vertical dashed line), while the onset of Z increase at NAQ is around 0237 UT. The onset of the particle injection, which is seen only in the electron data of 1982-019, is at 0244 UT (third vertical dashed line).

In Figure 14 we compare the onset time of high-speed ion flow, substorm current system, Pi 2 pulsations, and oscillations and compressional pulses in the inner magnetosphere. The first Pi 2 pulsation is observed at HER (3.1 MLT) at 0236:30 UT (the leftmost vertical dashed line) and slightly later at OTT (21.6 MLT). Magnetic oscillations start at ISEE 1 around this time. Then, three compressional pulses are observed by AMPTE/CCE at 2.1 MLT, as shown by the three vertical dashed lines. These compressional pulses are clearly accompanied by the second, third, and fourth Pi 2 wave packets observed at OTT. They are also accompanied by the three decreases of H at NAQ. It is interesting to note that the first and the second compressional pulses at AMPTE/CCE occur just after the first and second high-speed flow bursts (0238–0242 UT and 0245–0246 UT) at AMPTE/IRM, respectively.

There are four Pi 2 wave packets during this substorm event. The first Pi 2 at 0237 UT is accompanied by the onset of Z increase at NAQ (0.6 MLT). Other signatures of the substorm current wedge are not seen in the midlatitude ground stations at this time. The characteristics of the first Pi 2 in the hodogram of Figure 9 are clearly different from those of the other three Pi 2. Probably the first Pi 2 onset is a "pseudo onset" which does not cause any distinct substorm signatures on the global scale.

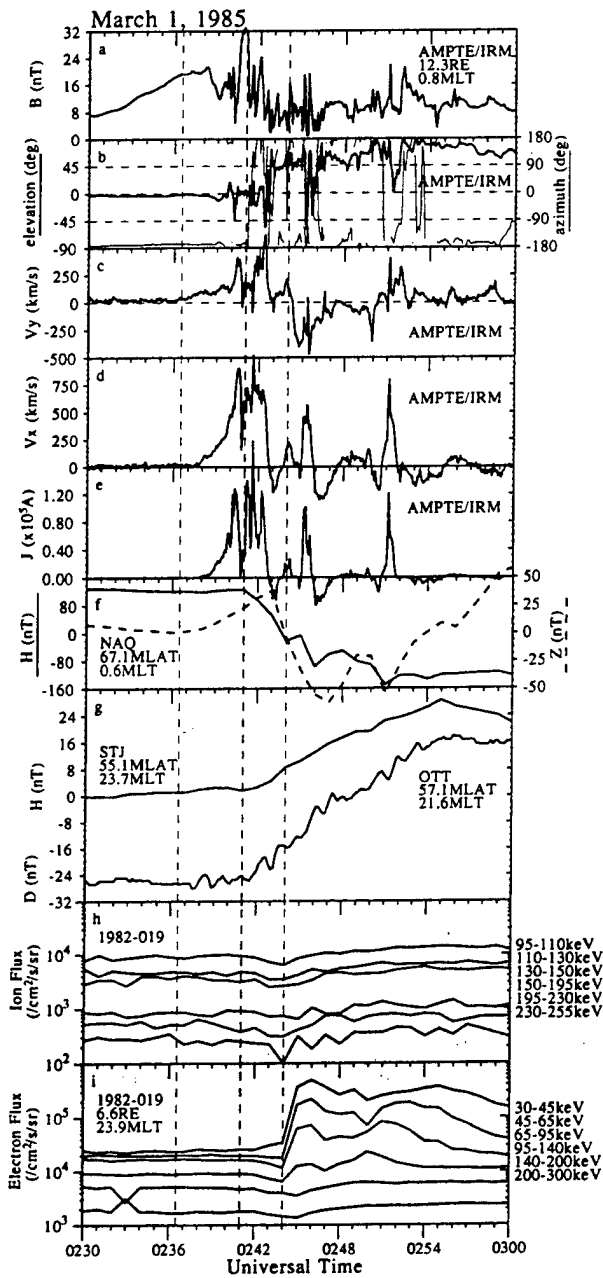


Figure 13. Comparison of the onset timings of high-speed ion flow in the near-Earth tail, ground signatures of westward electrojet and substorm current wedge, and particle injections at geosynchronous orbit, in the midnight sector. Three vertical dashed lines from left to right indicate the onset time of the first Pi 2 pulsation observed at HER at 0236:30 UT, that of westward electrojet and current wedge observed by ground stations, and that of particle injection observed by the 1982-019 satellite at 6.6 R_E , respectively. Figure 13e shows inertia current intensity estimated from the AMPTE/IRM measurement of the flow (see text for detail). The measurements by AMPTE/IRM are at 5-s resolution. The magnetic field data at OTT are at 10-s resolution. Other measurements of ground magnetic field and particle injection are at 1 min resolution. The MLT of ground stations and satellite footprints are those at 0240 UT.

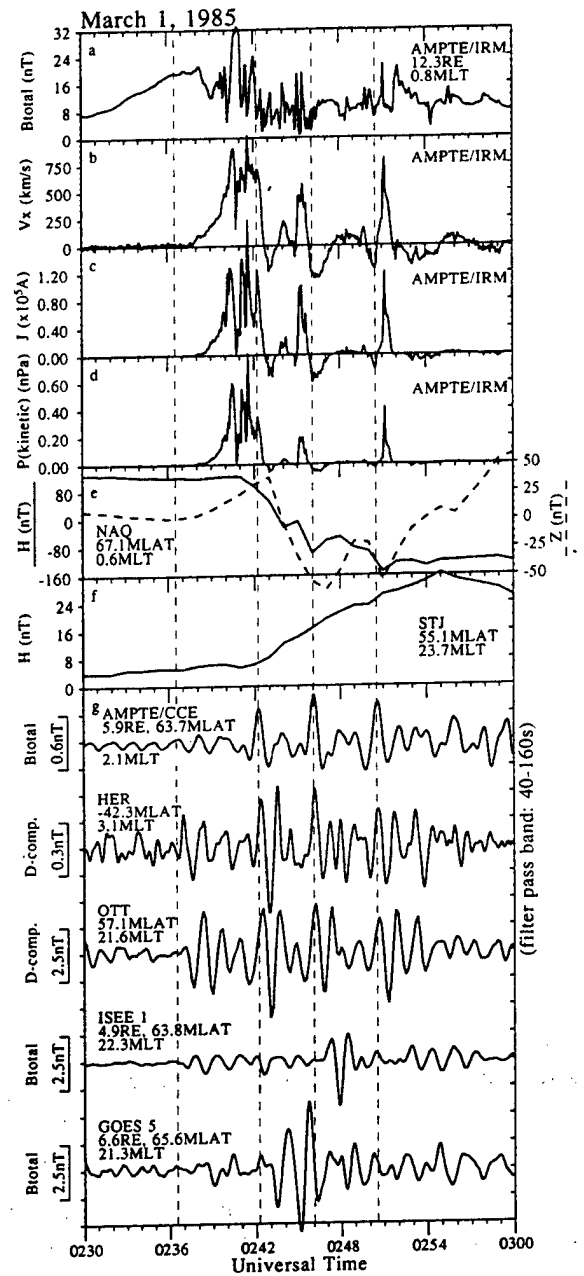


Figure 14. Comparison of the high-speed ion flow in the near-Earth tail, westward electrojet in the auroral zone, and Pi 2 magnetic pulsations and compressional pulses observed at ground stations and satellites in the inner magnetosphere. The leftmost vertical dashed line indicates the onset time of the first Pi 2 pulsation observed at HER, while the other three vertical lines indicate the peaks of the compressional pulses observed by AMPTE/CCE. Figures 14c and 14d show inertia current intensity and earthward kinetic pressure estimated from the AMPTE/IRM measurement of the flow. The MLT of ground stations and satellite footprints are those at 0240 UT.

On the other hand, the second Pi 2 at 0241 UT is accompanied by the clear onsets of negative H bay at NAQ, positive H bay at STJ (23.7MLT), and positive D enhancement at OTT (21.6MLT). It is quite conceivable that the second Pi 2 onset is the onset of the substorm current wedge on the global scale. Then, it is very interesting to note that the start of the high-speed flow at AMPTE/IRM is before the global onset of the substorm current wedge at 0241 UT.

There have been many multi-instrument studies of substorms which suggest the formation of the near-Earth neutral line [e.g., *McPherron and Manka*, 1985; *Lopez et al.*, 1990; *Kettmann et al.*, 1990; *Angelopoulos et al.*, 1996], while only a few papers have focused on the timing differences between the high-speed flow onset and the current wedge onset. *Angelopoulos et al.* [1994b] and *Sergeev et al.* [1995] have pointed out a delay of ground-based substorm signatures from a tailward flow onset, which is similar to the delay reported in this paper, on the basis of observations of a substorm event on April 15, 1979, by the ISEE 1 and 2 satellites (at about $16 R_E$ downtail). They explained that this timing difference is caused by the slow reconnection process on closed field lines during the substorm growth phase, on the basis of the conjectures by *Baker and McPherron* [1990] and *Baker et al.* [1993]. Here we propose an alternative model of the substorm expansion onset on the basis of previous work in which the braking of the earthward high-speed flow is considered to be the cause of the current wedge [*Hasegawa*, 1979; *Hesse and Birn*, 1991; *Haerendel*, 1992; *Shiokawa et al.*, 1997]. The model is also able to account for various observed substorm signatures in Figures 13 and 14. A schematic picture is shown in Figure 15 which will be described in the following subsections.

7.1. Relation of High-Speed Flow, Current Wedge, and Particle Injection

The X type reconnection in the near-Earth neutral line produces earthward ion flow earthward of the neutral line. The flow travels in the neutral sheet and is suddenly braked at the boundary between the dipolar and tail-like magnetic field because of the tailward pressure force, as suggested by *Shiokawa et al.* [1997]. The transition from a tail-like to a dipolar field configuration is formed by a dawnward inertia current at the boundary, which is caused by the deceleration of earthward high-speed ion flow [*Haerendel*, 1992]. The boundary moves tailward because of the pileup of the northward magnetic fluxes carried by the flow. In Figure 13 the

earthward high-speed flow from 0238 UT stops suddenly when the field becomes dipolar at 0242:30 UT. Also, after this time the earthward flow bursts are observed only when the field becomes tail-like (0245 and 0251 UT). These facts support the idea that AMPTE/IRM enters a region inside of the braking point when the field becomes dipolar. *Sergeev and Kubyskhina* [1996] also suggested, on the basis of particle data obtained by ionospheric satellites at a substorm onset, that the transition from tail-like to dipolar field configurations occurs within a distance of $0.5 R_E$.

The dawnward inertia current can be the cause of what is commonly named the tail current disruption, as suggested and quantitatively checked by *Haerendel* [1992]. Consequently, it separates the region of current disruption, i.e., generation of eastward current, from the reconnection or earthward flow acceleration region. The inconsistency between the location of current disruption (inside $15 R_E$, e.g., *Ohtani et al.* [1988]) and the location of the source of the flow (outside $20 R_E$, e.g., *Baumjohann et al.* [1990]) can be explained by this model.

There is an important difference between our model and that of current disruption. The latter suggests a diversion of the cross-tail current because of enhanced resistivity [*Lui et al.*, 1988] or some equivalent obstacle to the current flow. Our model is entirely related to the plasma dynamics.

At the braking point of the flow, two sources of the field-aligned current can be considered: (1) divergence of the dawnward inertia current [*Haerendel*, 1992] and (2) shear of the flow velocity at dawnside and duskside edges of the flow region [*Hasegawa*, 1979]. Note that the dawnward current due to the pileup of the northward magnetic flux cannot exceed the dawnward inertia current and should be handled as the same current perpendicular to the magnetic field in the MHD equations. *Hesse and Birn* [1991] noted from their 3-D MHD simulation that the current due to flow shear is more important than the current due to the flux pileup.

Shiokawa et al. [1997] have shown from a statistical study of high-speed flows observed by the AMPTE/IRM satellite that the average value of the inertia current and the current due to the flux pileup is $\sim 10^5$ A. In Figure 13e we show the inertia current estimated from the observed flow velocities and densities with the same assumption as that made by *Shiokawa et al.* [1997], while the vertical scale of the flow region is assumed to be $1 R_E$. The estimated inertia current is again the order of 10^5 A. *Sergeev et al.* [1996] and *Cramoysan et al.* [1995] have shown using ground-based magnetic field data for

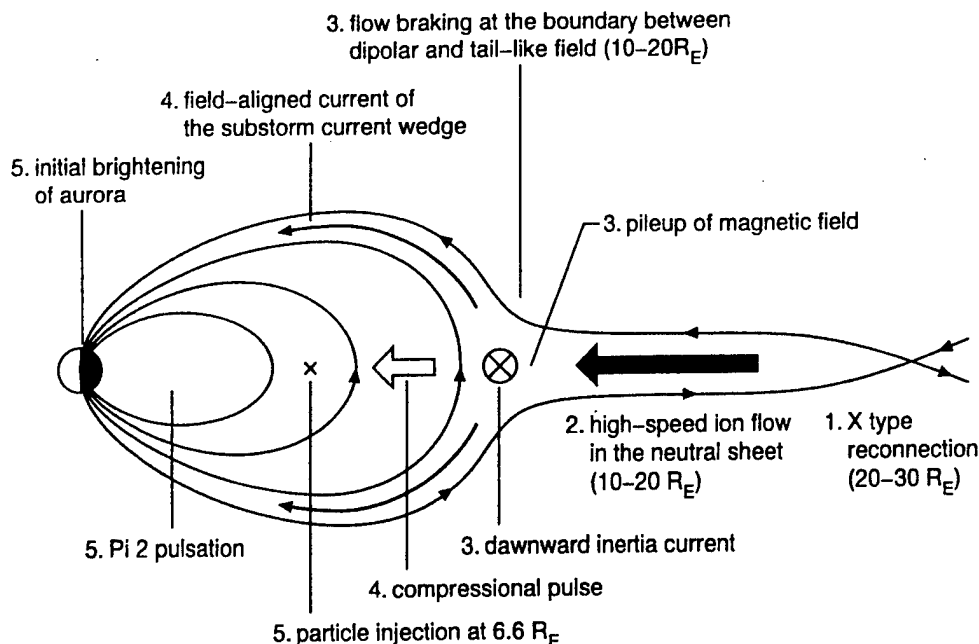


Figure 15. Proposed model of the current wedge formation during the initial stage of the substorm expansion phase. The number preceding each comment indicates the order of occurrence. The braking point of the earthward flow moves tailward because of the pileup of magnetic field carried by the flow. This motion probably corresponds to the poleward expansion of aurora. The transition from tail-like field to dipolar field at the braking point is due to the downward inertia current [Shiokawa *et al.*, 1997]. The substorm current wedge is formed at the braking point by the inertia current and the current due to flow shear. The fluctuation of field-aligned currents and the compressional pulses generated at the braking point can be the cause of the Pi 2 pulsation in the inner magnetosphere.

several substorm events that the total wedge current is typically $10^5 - 10^6$ A.

The field-aligned currents generated at the braking point of the flow are downward in the dawnside and upward in the duskside. The currents correspond to the substorm current wedge observed at ground-based stations. The initial brightening of aurora will occur at the ionospheric footprint of the upward field-aligned current region. This is consistent with previous observational facts that the typical locations of the initial brightening of aurora are mapped to the near-Earth tail at $|X| < 15 R_E$ [e.g., Murphree *et al.*, 1991]. The tailward motion of the braking point due to the pileup of the magnetic flux probably corresponds to the poleward expansion of aurora.

Angelopoulos *et al.* [1996] have concluded that the earthward energy transport by a flow event with a cross-sectional area of $\sim 15 R_E^2$ in the $Y-Z$ direction can account for the expected power consumption during a substorm event on April 11, 1985. We have made similar

analysis of the substorm energy budget for the present event with the same assumptions and equations as those used by Angelopoulos *et al.* [1996]. Assuming a cross-sectional area of $\sim 4 R_E^2$ in the $Y-Z$ direction, the earthward energy transport rate by the flow is consistent with the power consumption rate of the substorm (estimated from the *AE* and *Dst* indices) for 0240–0243 UT.

There is, however, an apparent inconsistency between the duration of the flow and of the substorm current system shown in Figure 13. The observed flow is bursty with a duration of only a few minutes, while the *H* bay at STJ and the *D* enhancement at OTT continue until 0255 UT. The westward electrojet current at NAQ reaches its maximum around this time. Probably, there is another source of the substorm current system during most of the expansion phase and the recovery phase.

Lopez *et al.* [1994] have pointed out that there are magnetic activities during which no high-speed flow is observed in the neutral sheet. Kamide and Kokubun [1996] have suggested two components of the auroral

electrojet currents due to directly driven and unloading processes in the solar wind-magnetosphere interactions. The event described by *Lopez et al.* [1994] may correspond to the magnetic activities caused by steady convection during the directly driven process. From these considerations we would like to limit the application of the model in Figure 15 to only the initial stage of the substorm expansion phase by the unloading process.

The observed difference of ~ 6 min between flow onset and the onset of high-energy particle injection shown in Figure 13 indicates that there is braking of the flow between $12 R_E$ and $6.6 R_E$ because the plasma in a high-speed flow event with a velocity of 400 km s^{-1} can travel $\sim 4 R_E$ per min. At the braking point of the flow, which is the boundary between dipolar and tail-like field regions, particles start drift motions in the dipolar background field. That means the braking point of the flow should correspond to the so-called "injection boundary," which is defined from high-energy particle observations at the geosynchronous orbit [*McIlwain*, 1974].

The $\mathbf{E} \times \mathbf{B}$ drift velocity \mathbf{v}_d is given by $|\mathbf{v}_d| = E/B$ where E is the intensity of duskward electric field. For $E = 1 \text{ mV m}^{-1}$ and $B = 10 \text{ nT}$ the earthward drift velocity $|\mathbf{v}_d|$ is 100 km s^{-1} ($\sim 1 R_E \text{ min}^{-1}$). This value is roughly consistent with the time delay of particle injection from the flow onset observed in this paper.

It must be cautioned, however, from statistical studies, that the location of the injection boundary is usually well inside $10 R_E$ in the midnight sector [e.g., *McIlwain*, 1974], while the braking point of the high-speed flow is probably at a tailward distance of $10\text{--}20 R_E$ in normal cases of high-speed flow since the occurrence rate of the flow drops in this distance range [*Baumjohann et al.*, 1990]. This mismatch should be explained in the future.

Magnetic field direction and intensity fluctuate strongly during the high-speed flow for 0239–0247 UT as shown in Figure 13a and 13b. The field sometimes becomes southward. These features are quite similar to those observed by the AMPTE/CCE satellite at $8\text{--}9 R_E$ [e.g., *Takahashi et al.*, 1987; *Lui et al.*, 1988]. On the basis of these observations, *Lui* [1991a, 1991b] proposed the current disruption model to explain the substorm expansion onset.

However, the magnetic fluctuations in Figure 13 may be caused by plasma instabilities associated with the high-speed flow and its braking. *Bauer et al.* [1995a] have shown statistically, using AMPTE/IRM observations, that high-speed flows are accompanied by intense fluctuations of magnetic field intensity. Any southward

directed field can be caused by turbulence in the neutral sheet since the braking point of the flow corresponds to the inner edge of the neutral sheet.

7.2. Relation Between High-Speed Ion Flow and Pi 2 Pulsations

It is interesting to note that three compressional pulses are observed by AMPTE/CCE at 2.1 MLT, as shown by the vertical dashed lines in Figure 14. These compressional pulses are clearly accompanied by the second, third, and fourth Pi 2 wave packets observed at HER and OTT. They are also accompanied by the decreases of H at NAQ, which indicate intensification of the westward electrojet current.

The first and the second compressional pulses at AMPTE/CCE occur just after the first and second high-speed flow bursts (0238–0242 UT and 0245–0246 UT) at AMPTE/IRM, respectively. The enhancement of earthward kinetic pressure due to the flow burst can cause compression of the inner magnetosphere at the braking point of the flow, as shown in Figure 15. The kinetic pressure is shown in Figure 14d. It is quite likely that the first and second compressional pulses observed at AMPTE/CCE are caused by the flow bursts observed at AMPTE/IRM. Note that this implies that the burstiness of the flow is caused by a temporal effect rather than a satellite motion in the spatial structure of flow layers.

It must be noted, however, that for a typical fast-mode Alfvén velocity of 1000 km s^{-1} ($10 R_E \text{ min}^{-1}$) as the travel speed of the compressional pulses in the magnetosphere, the delay time between the pulse observed at $6 R_E$ (AMPTE/CCE) and the flow burst at $12 R_E$ (AMPTE/IRM) should be only ~ 0.6 min. The first peak of the compressional pulse is delayed ~ 2 min from the first flow maximum. *Angelopoulos et al.* [1992] have suggested that the region of high-speed flow is quite localized in Y and Z . Thus the observed long delay of the first pulse may be due to the local time difference between AMPTE/IRM (0.8 MLT) and AMPTE/CCE (2.1 MLT). The third compressional pulse is observed just before the third flow burst at 0251 UT. This discrepancy may be also attributed to the same local time effect.

As discussed in the previous section, the high-speed flow produces field-aligned currents at its braking point. The estimated inertia current in Figure 14 shows large fluctuations with a time period of >1 min, suggesting the fluctuation of the induced field-aligned current. The kinetic pressure enhancement caused by the flow produces a compression of the inner magnetosphere as dis-

cussed above. Both effects can be the cause of the Pi 2 magnetic pulsation in the inner magnetosphere.

Bauer et al. [1995b] suggested neutral sheet oscillations during high-speed flows on the basis of AMPTE/IRM observations. The event shown in the present paper was also analyzed by them. They show that the correlation between the changes of the vertical velocity of the neutral sheet and thermal and magnetic pressure fluctuations is not good in the case of this event. This suggests that the flow fluctuations presented here are not spatial effects caused by neutral sheet oscillations.

The first Pi 2 at 0237 UT is not accompanied by any high-speed flow at AMPTE/IRM and compressional pulse at AMPTE/CCE. At the onset of the first Pi 2, magnetic field intensity at AMPTE/IRM stops to increase (Figure 13). This fact suggests that the pileup of lobe magnetic flux during substorm growth phase is stopped at this time.

The hodogram shown in Figure 9 indicates that the center of the Pi 2 current system for the first Pi 2 is likely to be westward from that of the second to fourth Pi 2. The first Pi 2 onset is probably caused by some processes that occur duskward of AMPTE/IRM (0.8MLT). That is why the compressional pulse is not observed at AMPTE/CCE (2.1MLT) only for the first Pi 2. Magnetic field oscillations are started at the same time as and at ~ 1 min after the first Pi 2 onset at ISEE 1 (Figure 12) and at AMPTE/CCE (Figure 10), respectively. These oscillations are probably caused by the same processes. It is difficult to discuss further the cause of the first Pi 2 onset using our limited data.

8. Conclusions

We have analyzed magnetic field and particle data obtained during an isolated substorm event on March 1, 1985, from many ground stations and satellites. The onset of the substorm current wedge in the midnight sector can be identified from the dense network of ground-based stations. AMPTE/IRM observed a clear onset of high-speed ion flow in the midnight sector at 12 R_E . The onset of the flow is observed 3 min before the onset of the global current wedge formation and 6 min before the onset of high-energy particle injection. On the basis of these observations we propose a model of the formation of current wedge during the initial stage of the substorm expansion phase (Figure 15). The wedge current is generated by processes at the braking point of the earthward high-speed flow. Hence this model separates the source region of the wedge current from the near-Earth neutral line. The problems which the near-

Earth neutral line model had faced [e.g., McPherron, 1995] can be solved by this model.

It is noted, however, that the application of this model should be limited only to the initial stage of the substorm expansion phase since the duration of high-speed flow is only a few minutes. Some additional process that causes the substorm current system probably comes into play during most of the expansion phase.

The proposed model also suggests that the compressional pulses and the fluctuations of field-aligned currents generated at the braking point of the flow are the initial cause of the Pi 2 magnetic pulsation in the inner magnetosphere. The good correspondence among three flow bursts at AMPTE/IRM, three compressional pulses at AMPTE/CCE, and three Pi 2 wave packets at ground stations during the substorm expansion phase supports this idea. Our observation also suggests the occurrence of a Pi 2 pulsation associated with a pseudo breakup that occurs at the late growth phase of the substorm. The source of the pseudo breakup Pi 2 is located in the different local time sector compared to that of the following global substorm onset.

References

- Akasofu, S.-I., Magnetospheric substorm, a model, *Solar Terrestrial Physics, Part III*, edited by D. Dyer, pp. 131, D. Reidel, Norwell, Mass., 1972.
- Angelopoulos, V., The role of impulsive particle acceleration in magnetotail circulation, *Proc. of the Third International Conference on Substorms (ICS-3)*, Eur. Space Agency, Versailles, France, 17-22, 1996.
- Angelopoulos, V., W. Baumjohann, C. F. Kennel, F. V. Coroniti, M. G. Kivelson, R. Pellat, R. J. Walker, H. Lühr, and G. Paschmann, Bursty bulk flows in the inner central plasma sheet, *J. Geophys. Res.*, **97**, 4027-4039, 1992.
- Angelopoulos, V., C. F. Kennel, F. V. Coroniti, R. Pellat, M. G. Kivelson, R. J. Walker, C. T. Russell, W. Baumjohann, W. C. Feldman, and J. T. Gosling, Statistical characteristics of bursty bulk flow events, *J. Geophys. Res.*, **99**, 21,257-21,280, 1994a.
- Angelopoulos, V., V. A. Sergeev, D. N. Baker, D. G. Mitchell, G. D. Reeves, C. T. Russell, and H. J. Singer, Multipoint study of bursty bulk flow events during a sequence of small substorms, *Proc. of the Second International Conference on Substorms (ICS-2)*, Univ. of Alaska, Fairbanks, Alaska, 643-650, 1994b.
- Angelopoulos, V., et al., Multipoint analysis of a bursty bulk flow event on April 11, 1985, *J. Geophys. Res.*, **101**, 4967-4989, 1996 (Correction, *J. Geophys. Res.*, **102**, 211-212, 1997).
- Baker, D. N., and R. L. McPherron, Extreme energetic particle decreases near geostationary orbit: A manifestation of current diversion within the inner plasma sheet, *J. Geophys. Res.*, **95**, 6591-6599, 1990.

- Baker, D. N., T. I. Pulkkinen, R. L. McPherron, J. D. Craven, L. A. Frank, R. D. Elphinstone, J. S. Murphree, J. F. Fennell, R. E. Lopez, and T. Nagai, CDAW 9 analysis of magnetospheric events on May 3, 1986: Event C, *J. Geophys. Res.*, **98**, 3815-3834, 1993.
- Bauer, T. M., W. Baumjohann, R. A. Treumann, N. Sckopke, and H. Lühr, Low-frequency waves in the near-Earth plasma sheet, *J. Geophys. Res.*, **100**, 9605-9617, 1995a.
- Bauer, T. M., W. Baumjohann, and R. A. Treumann, Neutral sheet oscillations at substorm onset, *J. Geophys. Res.*, **100**, 23,737-23,742, 1995b.
- Baumjohann, W., G. Paschmann, and C. A. Cattell, Average plasma properties in the central plasma sheet, *J. Geophys. Res.*, **94**, 6597-6606, 1989.
- Baumjohann, W., G. Paschmann, and H. Lühr, Characteristics of high-speed ion flows in the plasma sheet, *J. Geophys. Res.*, **95**, 3801-3809, 1990.
- Cramoysan, M., R. Bunting, and D. Orr, The use of a model current wedge in the determination of the position of substorm current systems, *Ann. Geophys.*, **13**, 583-594, 1995.
- Fairfield, D. H., A statistical determination of the shape and position of the geomagnetic neutral sheet, *J. Geophys. Res.*, **85**, 775-780, 1980.
- Fairfield, D. H., and N. F. Ness, Configuration of the geomagnetic tail during substorms, *J. Geophys. Res.*, **75**, 7032-7047, 1970.
- Haerendel, G., Disruption, Ballooning or auroral avalanche - on the cause of substorms, *Proc. of the First International Conference on Substorms (ICS-1)*, Eur. Space Agency, Kiruna, Sweden, 417-420, 1992.
- Hasegawa, A., Generation of field aligned current during substorm, in *Dynamics of the Magnetosphere*, edited by S.-I. Akasofu, pp. 529-542, D. Reidel, Norwell, Mass., 1979.
- Hesse, M., and J. Birn, On dipolarization and its relation to the substorm current wedge, *J. Geophys. Res.*, **96**, 19,417-19,426, 1991.
- Jacquey, C., J. A. Sauvaud, and J. Dandouras, Location and propagation of the magnetotail current disruption during substorm expansion: Analysis and simulation of an ISEE multi-onset event, *Geophys. Res. Lett.*, **18**, 389-392, 1991.
- Kamide, Y., and S. Kokubun, Two-component auroral electrojet: Importance for substorm studies, *J. Geophys. Res.*, **101**, 13,027-13,046, 1996.
- Kettmann, G., T. A. Fritz, and E. W. Hones Jr., CDAW 7 revisited: Further evidence for the criterion of a near-Earth neutral line, *J. Geophys. Res.*, **95**, 12,045-12,056, 1990.
- Lester, M., W. J. Hughes, and H. J. Singer, Polarization patterns of Pi 2 magnetic pulsations and the substorm current wedge, *J. Geophys. Res.*, **88**, 7958-7966, 1983.
- Lester, M., W. J. Hughes, and H. J. Singer, Longitudinal structure in Pi 2 pulsations and the substorm current wedge, *J. Geophys. Res.*, **89**, 5489-5494, 1984.
- Lopez, R. E., H. Lühr, B. J. Anderson, P. T. Newell, and R. W. McEntire, Multipoint observations of a small substorm, *J. Geophys. Res.*, **95**, 18,897-18,912, 1990.
- Lopez, R. E., C. C. Goodrich, G. D. Reeves, R. D. Belian, and A. Taktakishvili, Midtail plasma flows and the relationship to near-Earth substorm activity: A case study, *J. Geophys. Res.*, **99**, 23,561-23,569, 1994.
- Lühr, H., N. Klockner, B. Oelschlagel, B. Hausler, and M. Acuña, The IRM fluxgate magnetometer, *IEEE Trans. Geosci. Remote Sens.*, **23**, 259-261, 1985.
- Lui, A. T. Y., A synthesis of magnetospheric substorm models, *J. Geophys. Res.*, **96**, 1849-1856, 1991a.
- Lui, A. T. Y., Extended consideration of a synthesis model for magnetospheric substorms, in *Magnetospheric Substorms*, *Geophys. Monogr. Ser.*, vol. 64, edited by J. R. Kan et al., pp. 43-60, AGU, Washington, D. C., 1991b.
- Lui, A. T. Y., R. E. Lopez, S. M. Krimigis, R. W. McEntire, L. J. Zanetti, and T. A. Potemra, A case study of magnetotail current sheet disruption and diversion, *Geophys. Res. Lett.*, **15**, 721-724, 1988.
- McIlwain, C. E., Substorm injection boundaries, in *Magnetospheric Physics*, edited by B. M. McCormac, pp. 143-154, D. Reidel, Norwell, Mass., 1974.
- McPherron, R. L., Magnetospheric dynamics, in *Introduction to Space Physics*, edited by M. G. Kivelson and C. T. Russell, pp. 400-458, Cambridge Univ. Press, New York, 1995.
- McPherron, R. L., and R. H. Manka, Dynamics of the 1054 UT March 22, 1979, substorm event: CDAW 6, *J. Geophys. Res.*, **90**, 1175-1190, 1985.
- McPherron, R. L., C. T. Russell, and M. P. Aubry, Satellite studies of magnetospheric substorms on August 15, 1968, 9, Phenomenological model for substorms, *J. Geophys. Res.*, **78**, 3131-3149, 1973.
- Murphree, J. S., R. D. Elphinstone, L. L. Cogger, and D. Hearn, Viking optical substorm signatures, in *Magnetospheric Substorms*, *Geophys. Monogr. Ser.*, vol. 64, edited by J. R. Kan et al., pp. 241-255, AGU, Washington, D. C., 1991.
- Nagai, T., An empirical model of substorm-related magnetic field variations at synchronous orbit, in *Magnetospheric Substorms*, *Geophys. Monogr. Ser.*, vol. 64, edited by J. R. Kan et al., pp. 91-95, AGU, Washington, D. C., 1991.
- Nakamura, M., G. Paschmann, W. Baumjohann, and N. Sckopke, Ion distributions and flows near the neutral sheet, *J. Geophys. Res.*, **96**, 5631-5649, 1991.
- Ohtani, S., S. Kokubun, R. C. Elphic, and C. T. Russell, Field-aligned current signatures in the near-Earth tail region, 1, ISEE observations in the plasma sheet boundary layer, *J. Geophys. Res.*, **93**, 9709-9720, 1988.
- Ohtani, S., S. Kokubun, and C. T. Russell, Radial expansion of the tail current disruption during substorms: A new approach to the substorm onset region, *J. Geophys. Res.*, **97**, 3129-3136, 1992.
- Paschmann, G., H. Loidl, P. Obermayer, M. Ertl, R. Labrenz, N. Scopke, W. Baumjohann, C. W. Carlson, and D. W. Curtis, The plasma instrument for AMPTE/IRM, *IEEE Trans. Geosci. Remote Sens.*, **23**, 262-266, 1985.
- Potemra, T. A., L. J. Zanetti, and M. H. Acuña, The AMPTE CCE magnetic field experiments, *IEEE Trans. Geosci. Remote Sens.*, **GE-23**, 246-249, 1985.
- Russell, C. T., The ISEE-1 and ISEE-2 magnetometers, *Geosci. Electron.*, **16**, 239-242, 1978.
- Russell, C. T., and R. L. McPherron, The magnetotail and substorms, *Space Sci. Rev.*, **15**, 205-266, 1973.
- Saito, T., Geomagnetic pulsations, *Space Sci. Rev.*, **10**, 319-412, 1969.

- Sergeev, V. A., and M. V. Kubyshkina, Low altitude image of particle acceleration and magnetospheric reconfiguration at substorm onset, *J. Geomagn. Geoelectr.*, **48**, 877-885, 1996.
- Sergeev, V. A., V. Angelopoulos, D. G. Mitchell, and C. T. Russell, In situ observations of magnetotail reconnection prior to the onset of a small substorm, *J. Geophys. Res.*, **100**, 19,121-19,133, 1995.
- Sergeev, V. A., L. I. Vagina, R. D. Elphinstone, J. S. Murphy, D. J. Hearn, L. L. Cogger, and M. L. Johnson, Comparison of UV optical signatures with the substorm current wedge as predicted by an inversion algorithm, *J. Geophys. Res.*, **101**, 2615-2627, 1996.
- Shiokawa, K., W. Baumjohann, and G. Haerendel, Braking of high-speed flows in the near-Earth tail, *Geophys. Res. Lett.*, **24**, 1179-1182, 1997.
- Speiser, T. W., and R. F. Martin Jr., Remote sensing of the geomagnetic tail current sheet topology using energetic ions: Neutral lines versus weak field regions, *J. Geomagn. Geoelectr.*, **48**, 799-807, 1996.
- Takahashi, K., L. J. Zanetti, R. E. Lopez, R. W. McEntire, T. A. Potemra, and K. Yumoto, Disruption of the magnetotail current sheet observed by AMPTE/CCE, *Geophys. Res. Lett.*, **14**, 1019-1022, 1987.
- Takahashi, K., B. J. Anderson, and S. Ohtani, Multisatellite study of nightside transient toroidal waves, *J. Geophys. Res.*, **101**, 24,815-24,825, 1996.
- Tsyganenko, N. A., A magnetospheric magnetic field model with a warped tail current sheet, *Planet. Space Sci.*, **37**, 5-20, 1989.
- Yeoman, T. K., and D. Orr, Phase and spectral power of mid-latitude Pi 2 pulsations: Evidence for a plasmaspheric cavity resonance, *Planet. Space Sci.*, **37**, 1367-1383, 1989.
- Yumoto, K., Generation and propagation mechanisms of low-latitude magnetic pulsations - A review, *J. Geophys.*, **60**, 79-105, 1986.

TECHNOLOGY OPERATIONS

The Aerospace Corporation functions as an "architect-engineer" for national security programs, specializing in advanced military space systems. The Corporation's Technology Operations supports the effective and timely development and operation of national security systems through scientific research and the application of advanced technology. Vital to the success of the Corporation is the technical staff's wide-ranging expertise and its ability to stay abreast of new technological developments and program support issues associated with rapidly evolving space systems. Contributing capabilities are provided by these individual Technology Centers:

Electronics Technology Center: Microelectronics, VLSI reliability, failure analysis, solid-state device physics, compound semiconductors, radiation effects, infrared and CCD detector devices, Micro-Electro-Mechanical Systems (MEMS), and data storage and display technologies; lasers and electro-optics, solid state laser design, micro-optics, optical communications, and fiber optic sensors; atomic frequency standards, applied laser spectroscopy, laser chemistry, atmospheric propagation and beam control, LIDAR/LADAR remote sensing; solar cell and array testing and evaluation, battery electrochemistry, battery testing and evaluation.

Mechanics and Materials Technology Center: Evaluation and characterization of new materials: metals, alloys, ceramics, polymers and composites; development and analysis of advanced materials processing and deposition techniques; nondestructive evaluation, component failure analysis and reliability; fracture mechanics and stress corrosion; analysis and evaluation of materials at cryogenic and elevated temperatures; launch vehicle fluid mechanics, heat transfer and flight dynamics; aerothermodynamics; chemical and electric propulsion; environmental chemistry; combustion processes; spacecraft structural mechanics, space environment effects on materials, hardening and vulnerability assessment; contamination, thermal and structural control; lubrication and surface phenomena; microengineering technology and microinstrument development.

Space and Environment Technology Center: Magnetospheric, auroral and cosmic ray physics, wave-particle interactions, magnetospheric plasma waves; atmospheric and ionospheric physics, density and composition of the upper atmosphere, remote sensing, hyperspectral imagery; solar physics, infrared astronomy, infrared signature analysis; effects of solar activity, magnetic storms and nuclear explosions on the earth's atmosphere, ionosphere and magnetosphere; effects of electromagnetic and particulate radiations on space systems; component testing, space instrumentation; environmental monitoring, trace detection; atmospheric chemical reactions, atmospheric optics, light scattering, state-specific chemical reactions and radiative signatures of missile plumes, and sensor out-of-field-of-view rejection.